Title

Stereotactic Ablative Radiation Therapy Induces Systemic Differences in Peripheral Blood Immunophenotype Dependent on Irradiated Site

Journal

International Journal of Radiation Oncology • Biology • Physics, 101(5)

ISSN

0360-3016

Authors

McGee, Heather M

Daly, Megan E

Azghadi, Sohelia

et al.

Publication Date

2018-08-01

DOI

10.1016/j.ijrobp.2018.04.038

Peer reviewed

International Journal of Radiation Oncology biology • physics

www.redjournal.org

Biology Contribution

Stereotactic Ablative Radiation Therapy Induces Systemic Differences in Peripheral Blood Immunophenotype Dependent on Irradiated Site

Heather M. McGee, MD, PhD,[*,†] Megan E. Daly, MD,[*] Sohelia Azghadi, MD,[*] Susan L. Stewart, PhD,[‡] Leslie Oesterich, MD,[§] Jeffrey Schlom, PhD,[‖] Renee Donahue, PhD,[‖] Jonathan D. Schoenfeld, MD,[¶,#] Qian Chen, BS,[**] Shyam Rao, MD, PhD,[*] Ruben C. Fragoso, MD, PhD,[*] Richard K. Valicenti, MD,[*] Robert J. Canter, MD,[**] Emmanual M. Maverakis, PhD,[**] William J. Murphy, PhD,[**,††] Karen Kelly, MD,[§] and Arta M. Monjazeb, MD, PhD[*,**]

*[*]Department of Radiation Oncology and [§]Division of Medical Oncology, Department of Medicine, University of California, Davis, Comprehensive Cancer Center, Davis, California; [†]Department of Radiation Oncology, Icahn School of Medicine at Mount Sinai, New York, New York; [‡]Department of Public Health Sciences, **Laboratory of Cancer Immunology, and [††]Department of Dermatology, University of California, Davis, School of Medicine, Davis, California; [‖]Laboratory of Cancer Immunology and Biology, Center for Cancer Research, National Cancer Institute, National Institutes of Health, Bethesda, Maryland; [¶]Department of Radiation Oncology, Dana-Farber/Brigham and Women's Cancer Center, Boston, Massachusetts; and [#]Department of Radiation Oncology, Harvard Medical School, Boston, Massachusetts*

Received Nov 28, 2017, and in revised form Apr 7, 2018. Accepted for publication Apr 16, 2018.

Summary

We performed a prospective study to assess the systemic immune response 1 to

Purpose: Despite the strong interest in combining stereotactic ablative radiation therapy (SAR) with immunotherapy, limited data characterizing the systemic immune response after SAR are available. We hypothesized that the systemic immune response to SAR would differ by irradiated site owing to inherent differences in the microenvironment of various organs.

Reprint requests to: Megan E. Daly, MD, Department of Radiation Oncology, University of California, Davis, School of Medicine, 4501 X St, Sacramento, CA 95817. Tel: (916) 734-5428; E-mail: medaly@ucdavis.edu

H. M. McGee and M. E. Daly contributed equally to this work.

The present research was supported in part by the National Institutes of Health National Cancer Institute (award no. K12CA138464 to M.E.D.). This project was also supported by the University of California Davis Flow Cytometry Shared Resource Laboratory with funding from the National Cancer Institute (grant P30CA093373), National Institutes of Health National Center for Research Resources (grants C06-RR12088, S10 OD018223, S10 RR12964, and S10 RR 026825). The content is solely the responsibility of the authors and does not necessarily represent the official views of the National Institutes of Health.

Conflict of interest: H. McGee reports participation on the advisory board for AstraZeneca. M. Daly reports research funding from EMD Sereno. J. Schoenfeld reports research/clinical trial funding from Merck, Bristol Myers-Squibb, and Regeneron and participation on the advisory board for AstraZeneca, Bristol Myers-Squibb, Debiopharm, and Nanobiotix. A. Monjazeb reports research/clinical trial funding from Transgene, Incyte, Genentech, Merck, and EMD Serono and participation on the advisory board for AstraZeneca.

Supplementary material for this article can be found at www.redjournal.org.

Acknowledgments—We thank Jonathan Van Dyke and Laura Paige Olney for technical assistance and the University of California Davis Laboratory for Cancer Immunology for technical support.

Int J Radiation Oncol Biol Phys, Vol. 101, No. 5, pp. 1259–1270, 2018
0360-3016/$ - see front matter
https://doi.org/10.1016/j.ijrobp.2018.04.038

2 weeks after SAR to different organs using flow cytometry for immunophenotyping and Luminex analysis. Our results suggest that SAR to parenchymal sites (lung and liver) induces systemic immune changes, including a decrease in total and cytotoxic NK cells and an increase in TIM3$^+$ NK cells and activated memory CD4$^+$ and CD8$^+$ T cells. SAR to nonparenchymal sites did not induce these changes.

Methods and Materials: Patients receiving SAR to any organ underwent prospective blood banking before and 1 to 2 weeks after SAR. Peripheral blood mononuclear cells (PBMCs) and serum were isolated. PBMCs were stained with fluorophore-conjugated antibodies against T and natural killer (NK) cell markers. Cells were interrogated by flow cytometry, and the results were analyzed using FlowJo software. Serum cytokine and chemokine levels were measured using Luminex. We analyzed the changes from before to after therapy using paired *t* tests or 1-way analysis of variance (ANOVA) with Bonferroni's post-test.

Results: A total of 31 patients had evaluable PBMCs for flow cytometry and 37 had evaluable serum samples for Luminex analysis. The total number of NK cells and cytotoxic (CD56^{dim}CD16$^+$) NK cells decreased ($P = .02$) and T-cell immunoglobulin- and mucin domain−containing molecule-3−positive (TIM3$^+$) NK cells increased ($P = .04$) after SAR to parenchymal sites (lung and liver) but not to bone or brain. The total memory CD4$^+$ T cells, activated inducible co-stimulator−positive and CD25$^+$CD4$^+$ memory T cells, and activated CD25$^+$CD8$^+$ memory T cells increased after SAR to parenchymal sites but not bone or brain. The circulating levels of tumor necrosis factor-α ($P = .04$) and multiple chemokines, including RANTES ($P = .04$), decreased after SAR to parenchymal sites but not bone or brain.

Conclusions: Our data suggest SAR to parenchymal sites induces systemic immune changes, including a decrease in total and cytotoxic NK cells, an increase in TIM3$^+$ NK cells, and an increase in activated memory CD4$^+$ and CD8$^+$ T cells. SAR to nonparenchymal sites did not induce these changes. By comparing the immune response after radiation to different organs, our data suggest SAR induces systemic immunologic changes that are dependent on the irradiated site.

Introduction

Stereotactic ablative radiation therapy (SAR), a technique for delivering ablative doses of conformal radiation therapy (RT) over 1 to 5 fractions, has emerged as a standard treatment option for a variety of solid tumors, both for definitive therapy of localized disease and for local control of metastatic sites (1-7). Recently, considerable interest has ensued for combining RT with immunotherapy to use radiation as an *in situ* tumor vaccine that enhances the efficacy of immunotherapy (8-12). Although many registered, actively accruing clinical trials have incorporated radiation with immune checkpoint inhibitors (13, 14), it is unclear how to optimize the RT in these trials, because data investigating the immune response to SAR alone are insufficient.

The immunomodulatory effects of RT, in particular, the local immune effects on the tumor microenvironment, have been well-established in preclinical models (8, 15), and include induction of immunogenic cell death (16, 17), release of antigens for T-cell priming (18), improved T-cell homing to tumor sites (19), a shift in the polarization of tumor-associated macrophages (19), and destruction of immunosuppressive stromal cells in the tumor microenvironment (20), among others. The findings from more recent studies have suggested that hypofractionated radiation schedules produce very different biologic effects than traditional conventionally fractionated radiation schedules (21-24). Clinical reports of distant or "abscopal" responses in patients have described systemic immunophenotype changes; however, all these reports were in the setting of combined RT and immunotherapy (25-27). Several small studies have investigated the immune response to SAR for early-stage lung cancer (28, 29). More recently, additional studies have investigated components of the immune response after SAR for hepatocellular carcinoma (30), pancreatic cancer (31), and breast cancer (32). However, to the best of our knowledge, no studies have directly compared changes in systemic immunophenotype and cytokine signatures after SAR without systemic therapy to different irradiated sites. Investigating differences in systemic immunophenotype after SAR according to the irradiated site could be critical for the rational design of future combined SAR plus immunotherapy trials.

Well-defined, inherent differences exist in the immune microenvironment of different organs, from the relatively immunoprivileged brain protected by the blood−brain barrier and the immunoprivileged bone marrow to the immunotolerant lung and liver, which are constantly exposed to antigens (33-35). Because natural killer (NK) cells constitute a large portion of the immunotolerant organs such as the lung and liver, we hypothesized that radiation to these sites might cause unique changes in specific NK cell populations (33, 36). We hypothesized that the systemic immune response to SAR would differ by irradiated site and sought to gain a comprehensive understanding of these differences to refine future clinical trials combining

RT and immunotherapy. We prospectively collected blood samples before SAR and 1 to 2 weeks after SAR from patients undergoing SAR to the lung, liver, bone, or brain to measure the changes in markers of the systemic immune response, such as cytokine/chemokine signatures and immunophenotype changes in peripheral blood mononucleated cells (PBMCs).

Methods and Materials

Patients

Patients were recruited as part of an institutional review board-approved blood collection protocol at University of California, Davis, designed to assess the systemic immune response after SAR. Patients seen in the radiation oncology clinic in consultation for SAR were recruited by the study team investigators. Eligible patients were scheduled to undergo 1 to 5 fractions of stereotactic body RT (SBRT) or 1 to 10 fractions of hypofractionated conformal RT for cancer of any histologic type and site (including the lung, liver, adrenal, brain, or bone, and other organs) per standard-of-care treatment. Patients aged <18 years and those unable to provide informed consent were ineligible. No specific eligibility criteria regarding concurrent or previous systemic therapy were used. Blood samples were obtained by venipuncture before RT (at consultation, treatment simulation, or the first day of treatment before delivery of the first fraction) and 7 to 14 days after RT. For each blood sample, $\sim$30 mL of blood was collected in 10-mL vacutainer blood collection tubes with and without EDTA (for PBMCs and serum, respectively; Becton Dickinson, Franklin Lakes, NJ). All blood samples were de-identified before processing of serum and PBMCs.

Blood processing and Storage

Whole blood was centrifuged at 1400 rpm for 15 minutes at room temperature. Serum and plasma were separated into aliquots in cryovials to be frozen at -80°C. Mononuclear cells were isolated using Ficoll-Paque gradient (BD Biosciences). This was centrifuged at 1400 rpm for 5 minutes at room temperature. After red blood cell lysis, the PBMCs were counted for viability and resuspended in freezing medium (50% Iscove's modified Dulbecco's medium, 40% fetal bovine serum, and 10% dimethyl sulfoxide) at a concentration of 1 to 10×10^6 cells/mL. The cells were separated into aliquots in cryogenic vials and stored at -80°C in the Laboratory for Cancer Immunology, where testing was performed by study personnel.

Luminex analysis

Luminex bead-based assays (BioRad, Hercules, CA) were performed on serum specimens from 37 patients to measure circulating levels of 19 cytokines and 11 chemokines (Appendix E1; available online at www.redjournal.org) according to the manufacturer's instructions. Most cytokines were assessed using the Cytokine 17-plex assay (M5000031YV); however, cytokine interferon (IFN)-α2 (171B6010M) was measured using cytokine group II standards (171D6001). Transforming growth factor (TGF)-β isoforms 1, 2, and 3 were measured using the TGF-β1, -2, -3 kit (TGFBNAG-64K-03; EMD Millipore, Billerica, MA). Most of the chemokines were measured using the chemokine standard 171DK0001, and RANTES was measured with the standard 171B5025M. Concentrations were calculated using a 5-parameter standard curve. Serum samples were assayed in duplicate and averaged to calculate the final concentrations.

Flow cytometry

PBMCs were thawed rapidly in a 37°C water bath and diluted into RF10 media (Roswell Park Memorial Institute 1640 medium (Thermo Fischer Scientific) with 10% fetal bovine serum and 1% penicillin/streptomycin (Sigma-Aldrich). Cell number and viability were determined using trypan blue exclusion with a hemocytometer after thawing. The PBMCs from 30 patients were available for flow cytometry analysis. Immunophenotyping of PBMCs was performed using 2 panels of antibodies, 1 panel to characterize the NK cells and 1 to characterize the T cells (37, 38). All fluorochrome-conjugated antibodies (Appendix E2; available online at www.redjournal.org) were from BioLegend (San Diego, CA), unless otherwise indicated. The cells were incubated with antibodies diluted in staining buffer (phosphate-buffered saline containing 1% human serum and 1% penicillin/streptomycin) at 4°C in the dark for 20 minutes. Cells stained with the NK panel were washed, centrifuged, resuspended in staining buffer, and stored at 4°C. Cells stained with the T-cell panel were washed, fixed with Fix/Perm buffer (eBiosciences, San Diego, CA) for 30 minutes at 4°C. After washing, the cells were resuspended in Perm/Wash buffer containing anti-Foxp3 antibody or isotype control for 30 minutes in the dark at room temperature before being washed and resuspended in staining buffer. Phenotype analysis was performed by gating 50,000 to 200,000 cells according to forward scatter/side scatter with a LSR Fortessa flow cytometer using DIVA, version 6, software (BD Biosciences, San Diego, CA). Data were analyzed using FlowJo software (FlowJo LLC, Ashland, OR). The positive and negative cell populations for each marker were determined using fluorescence minus one controls (39), with unstained cells used as a negative control. Instrument settings were verified and adjusted with the mid-peak bead of the 8-peak calibration bead set (Spherotech) before each acquisition session. Compensation beads (BD Biosciences) were used to correct for spectral overlap between channels.

Statistical analysis

Statistical analyses were performed using GraphPad Prism software (GraphPad, La Jolla, CA) and R (R Foundation,

Vienna, Austria). The baseline characteristics between subgroups were compared using χ^2 tests and 1-way analysis of variance (ANOVA). The changes for each parameter across the entire cohort were assessed using paired *t* tests. To explore the differential response across treatment sites, lung and liver lesions were combined into 1 cohort as parenchymal sites. Differences in immunophenotype changes and cytokine/chemokine response between the parenchymal sites and bone and brain sites were analyzed using 1-way ANOVA with Bonferroni's post-test for continuous variables to account for multiple comparisons. χ^2 tests were used to identify significant variation across subgroups. Data are presented in bar graphs, with vertical bars indicating the mean and lines representing the standard error of the mean. Spearman's correlation coefficients were computed for changes in each immune cell population with radiation-associated variables, including total dose, dose per fraction, and size in cubic centimeters of the planning target volume (PTV). For all tests, statistical significance was assessed at the $P \leq .05$ level (2-sided).

Results

Patient characteristics

Patients scheduled to undergo SAR to any organ for a primary or metastatic solid tumor were prospectively enrolled in an institutional blood banking protocol from August 2014 to June 2017. A total of 40 patients were included in the analysis. Of these 40 patients, 31 had evaluable PBMC samples from before and 7 to 14 days after SAR, and 37 had pre- and post-treatment serum samples suitable for Luminex analysis of cytokines and chemokines. Of the 40 total patients included in either analysis, 22 (54%) had undergone SAR for a lung tumor, 4 (9.8%) had undergone SAR to a liver tumor, 9 (22.0%) had undergone SAR to a bone lesion, and 5 (12.2%) had undergone SAR to the brain. One patient (2.4%) was treated to both a lung tumor and soft tissue tumor simultaneously.

The baseline patient characteristics for all patients included in the immunophenotyping or Luminex analysis

Table 1 Patient characteristics

Characteristic	Parenchymal (lung and liver; n = 26)	Bone (n = 9)	Brain (n = 5)	*P* value
Age (y)				.13
Median	71	64	66	
Range	30-86	37-78	48-74	
PTV (cc)				.13
Median	31.3	48.9	0.8	
Range	5.5-277.8	11.5-174.1	0.6-2.1	
Disease stage				
I	20	0	0	
II	1	0	0	
IV	5	9	5	
Pack-year smoking				.17
Median	13	0	15	
Range	0-120	0-30	0-40	
Dose (Gy)				<.00001*
Median	50	24	21	
Range	35-54	24-27	20-21	
Fractions (n)				<.00001*
Median	5	3	1	
Range	3-5	3-3	1-1	
Histologic type				.46
Adenocarcinoma	12 (46)	7 (78)	2 (40)	
Squamous	5 (19)	0 (0)	1 (20)	
Sarcoma	3 (12)	0 (0)	0 (0)	
Undifferentiated/other	3 (12)	2 (22)	2 (40)	
Unbiopsied	3 (12)	0 (0)	0 (0)	
Previous systemic therapy (%)	38	78	60	.11
Cytotoxic chemotherapy	8	0	2	
Endocrine therapy†	0	3	1	
Immunotherapy	0	1	1	
Targeted therapy	2	3	0	

Abbreviations: Pack-years = number of pack-years of smoking cigarettes in the patient's lifetime; PTV = planning target volume.
Data presented as median and range, n (%), or %.
* Statistically significant.
† Endocrine therapy for metastatic prostate cancer.

are shown in Table 1. The median age was 68 years (range 37-86), with 23 men (58%) and 17 women (42%). A nonsignificant trend toward older median age and greater pack-year smoking history was noted for patients treated to parenchymal sites compared with those treated to brain or bone. Of the patients treated to parenchymal sites, 41% had received ≥1 previous course of chemotherapy in their lifetime compared with 60% to 66% of patients treated to bone or brain ($P = .35$). No enrolled patients were receiving systemic dose steroids or concurrent infusional chemotherapy or immunotherapy at the time of SBRT. Seven patients were receiving other cancer-directed systemic therapy at the time of SAR, including androgen deprivation (n = 1), endocrine (n = 2), tyrosine kinase inhibitor (n = 3), or oral capcitabine (n = 1) therapy. Twenty-four patients had not received cancer-directed systemic therapy within the previous year. Among the remaining 9 patients who had received systemic therapy within the previous year, the median time from the last systemic therapy was 74 days (range 14-254). The median PTV was 29.4 cm^3 (range 5.5-118.1) for parenchymal lesions, 48.9 cm^3 (range 11.5-137) for bone lesions, and 0.84 cm^3 (range 0.06-2.08) for brain lesions ($P = .13$). The parenchymal group received a median dose of 50 Gy (range 35-54) over 3 to 5 fractions, the bone group received a median dose of 24 Gy (range 24-27) over 3 fractions, and the brain group received a median of 21 Gy (range 20-21) in a single fraction ($P < .001$). However, the groups were similar in terms of the other patient characteristics (Table 1).

Changes in NK cells in the periphery after SAR to parenchymal sites

PBMCs from 31 patients were available for flow cytometry analysis. Surface staining of NK cell markers was used in the gating strategy to identify NK cell subsets (Fig. 1A). A statistically significant decrease was found in the percentage of total NK cells after SAR to the parenchymal sites (20.49 ± 2.36 vs 16.76 ± 2.436; $P = .01$; Fig. 1B; Fig. E1A; available online at www.redjournal.org). In addition, a significant decrease occurred in the percentage of cytotoxic $CD56^{dim}CD16^{+}$ NK cells after SAR to the parenchymal sites (17.58 ± 2.34 vs 13.17 ± 2.052; $P = .024$; Fig. 1C). No significant change was identified in the percentage of cytokine-producing $CD56^{high}CD16^{-}$ NK cells in the periphery for any patient cohort. No statistically significant change was found in the percentage of total NK cells, cytotoxic NK cells, or cytokine-producing NK cells

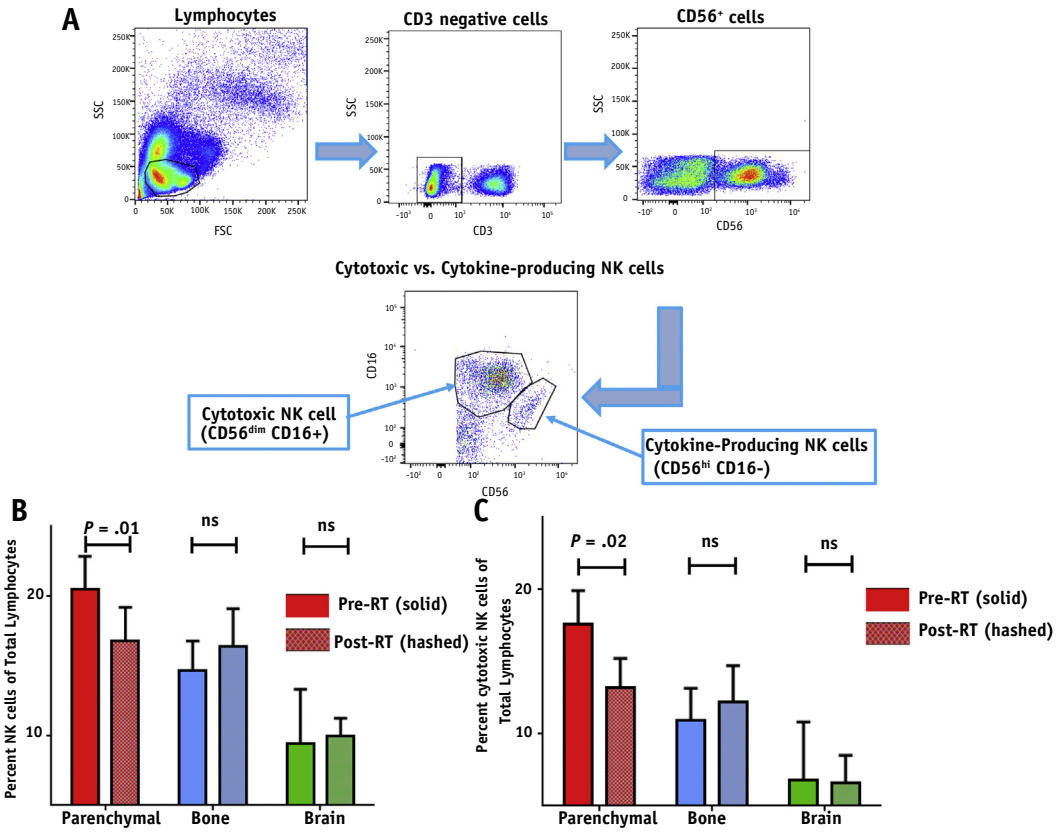

Fig. 1. Decrease in the percentage of total and cytotoxic natural killer (NK) cells after stereotactic ablative radiation therapy (RT; SAR) to parenchymal sites but not bone or brain. (A) Gating strategy for identification of NK cell subsets from total lymphocytes in peripheral blood mononuclear cells (PBMCs). (B) Percent of total NK cells in PBMCs after SAR to parenchymal sites, bone, and brain. (C) Percent of cytotoxic NK cells in PBMCs after SAR to parenchymal sites, bone, and brain.

after SAR to the bone or brain (Fig. 1B; Fig. E1B, C; available online at www.redjournal.org). In addition, we identified a statistically significant increase in the percentage of T-cell immunoglobulin- and mucin domain–containing molecule-3–positive ($TIM3^+$) NK cells in the peripheral blood after SAR to the parenchymal sites (15.84 ± 3.165 vs 19.65 ± 3.261; $P = .039$) but not after SAR to the bone or brain (Fig. 2). No statistically significant difference was identified in programmed cell death 1 (PD-1) expression on any NK cell subset after SAR (data not shown).

Increase in activated memory $CD4^+$ and $CD8^+$ T cells after SAR to parenchymal sites

Human naive and memory T cells are distinguished by CD45RA and CD45RO reciprocal isoforms (40), and central and effector memory T-cell subsets were identified by the expression of CD45R isoforms and either of the homing molecules, CCR7 or CD62L (41). In the present study, we designated $CD45RA^-CD62L^+$ T cells to represent central memory T cells (which home to the lymph nodes) and $CD45RA^-CD62L^-$ cells to represent effector memory T cells (which perform effector functions in the tissue) (41) (Fig. 3A). A statistically significant increase was found in the percentage of total $CD4^+$ memory T cells in the PBMCs after SAR to the parenchymal sites (29.68 ± 2.65 vs 38.75 ± 3.46; $P = .026$; Fig. 3B; Fig. E2A; available online at www.redjournal.org) but not after SAR to the bone or brain (Fig. 3B; Fig. E2B, C; available online at www.redjournal.org).

Our analysis of the effector and central memory $CD4^+$ T-cell compartments focused on the expression of the activation markers, CD25 and inducible co-stimulator (ICOS), on memory T-cell subsets (Fig. 3C, D). We identified an increase in the percentage of activated $CD4^+$ memory T cells after SAR as demonstrated by a marked increase in the percentage of $ICOS^+CD4^+$ T cells of total lymphocytes (0.8813 ± 0.19 vs 1.739 ± 0.241; $P = .0005$; Fig. 3C) and about a twofold increase in the percentage of activated $CD25^+CD4^+$ T cells after SAR (1.414 ± 0.42 vs 2.97 ± 0.60; $P = .078$; Fig. 3D). None of these changes were seen after SAR to the bone or brain (Fig. 3C, D). No change in PD-1 expression was seen in the memory $CD4^+$ T-cell population after SAR to any site (Fig. E3; available online at www.redjournal.org). In addition, the percentage of $CD25^+Foxp3^+CD4^+$ regulatory T cells did not change after SAR to any site (Fig. E4; available online at www.redjournal.org).

Analysis of $CD8^+$ memory T cells showed no difference in the percentage of total $CD8^+$ T cells after SAR (Fig. 4A) but did show a strong trend toward an increase in the percentage of activated $CD25^+CD8^+$ memory T cells after SAR to the parenchymal sites (1.388 ± 0.49 vs 3.50 ± 1.10; $P = .058$; Fig. 4B). No changes were seen in the $CD8^+$ memory T-cell populations after SAR to the bone or brain.

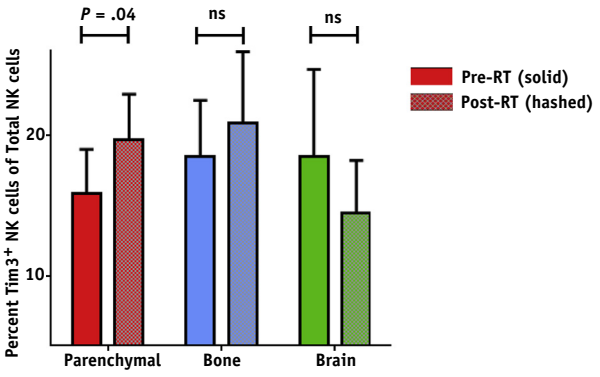

Fig. 2. Increase in percentage of T-cell immunoglobulin- and mucin domain–containing molecule-3-positive ($TIM3^+$) natural killer (NK) cells after stereotactic ablative radiation therapy (RT; SAR) to parenchymal sites. Percentage of $TIM3^+$ NK cells of the total NK cell population in peripheral blood mononuclear cells after SAR to parenchymal sites (red), bone (blue), and brain (green). (A color version of this figure is available at www.redjournal.org.).

Effect of total dose, dose per fraction, and PTV on immune cell populations

The total dose was positively associated with the change in the percentage of $ICOS^+CD4^+$ memory T cells (Spearman's correlation coefficient $\rho = 0.46$; $P = .022$) and change in the percentage of $CD25^+CD8^+$ memory T cells ($\rho = 0.57$; $P = .006$). The dose per fraction was not associated with any changes in the immune cell populations (Table E1; available online at www.redjournal.org). The PTV size was positively associated with the change in the percentage of $ICOS^+CD4^+$ memory T cells ($\rho = 0.43$; $P = .031$) and the change in the percentage of T regulatory cells ($\rho = 0.43$; $P = .031$). In addition, PTV size was associated with the change in the percentage of $TIM3^+$ NK cells ($\rho = 0.48$; $P = .008$; Table 1; available online at www.redjournal.org).

Changes in cytokine and chemokines after SAR to parenchymal sites

Serum specimens from 37 patients were evaluable for Luminex analysis. We measured the circulating levels of 19 cytokines and 11 chemokines (Appendix E1; available online at www.redjournal.org). Those cytokines and chemokines with >75% of values less than the lowest limit of detection were excluded from the present analysis. Therefore, the final Luminex analysis included 15 evaluable markers (interleukin [IL]-2, IL-4, IL-6, IL-12, TGF-β1, TGF-β2, tumor necrosis factor [TNF]-α, inducible protein 10 (IP-10), RANTES, MIP-1α, MIP-1β, MCP1,

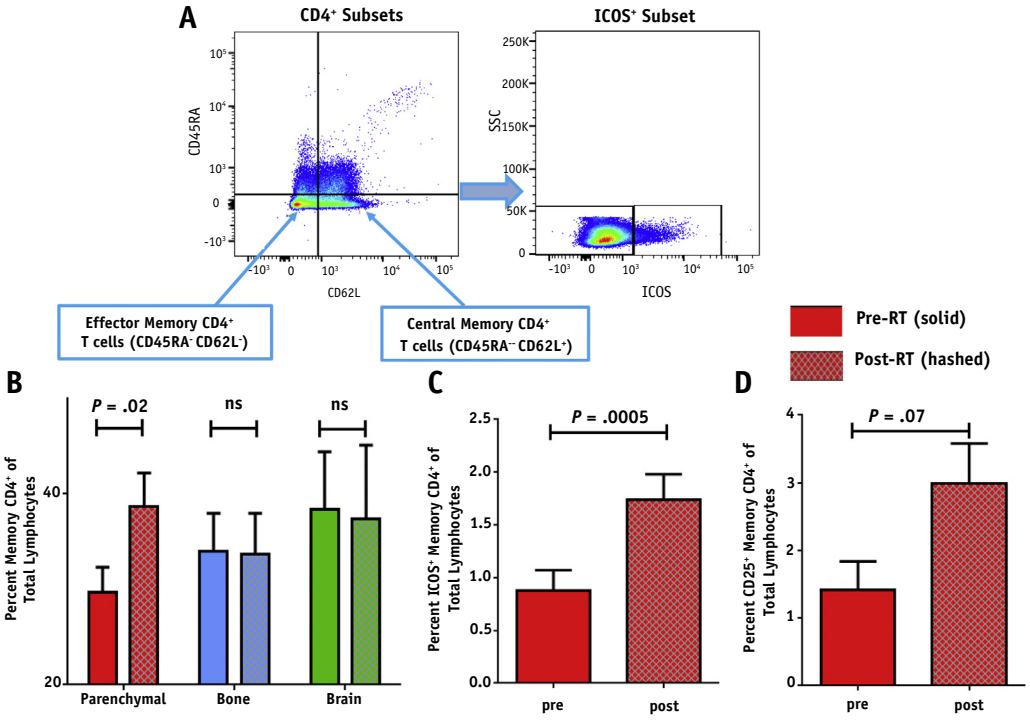

Fig. 3. Stereotactic ablative radiation therapy (RT; SAR) causes increases in percentage of memory $CD4^+$ and $CD8^+$ T-cell populations, including activated inducible costimulatory-positive ($ICOS^+$) and $CD25^+$ memory T cells. (A) Gating strategy for memory $CD4^+$ T-cell subsets and activated $ICOS^+$ cells. (B) Percent of memory $CD4^+$ T-cell populations after SAR to parenchymal organs, bone, and brain. (C) Percent of activated $ICOS^+$ $CD4^+$ memory T-cell population after SAR to parenchymal sites alone. (D) Percent of activated $CD25^+$ memory $CD4^+$ T-cell populations after SAR to parenchymal sites alone.

MCP2, and SCYB16). A systemic decrease occurred in TNF-α (23.10 ± 1.97 vs 19.54 ± 1.797; $P = .042$), and the chemokines IP-10 (459.4 ± 79.76 vs 347.8 ± 44.75; $P = .048$), MCP1 (14.4 ± 0.96 vs 11.55 ± 1.00; $P = .0098$), MCP2 (172.5 ± 18.54 vs 138.6 ± 12.43; $P = .007$), MIP-1α (18.67 ± 1.49 vs 16.33 ± 1.32; $P = .024$), and RANTES (9028 ± 864.8 vs 6759 ± 485.3; $P = .035$) after SAR to the parenchymal sites (Fig. 5). Bonferroni's correction was used to correct for multiple hypothesis testing. No significant cytokine changes were observed after SAR to the bone or brain (Fig. 5). No changes in the pro-inflammatory cytokines IFN-α, IFN-γ, or TGF-β were identified.

Discussion

Owing to widespread interest in combining RT with immunotherapy, numerous actively accruing clinical trials are underway that combine SAR with immune checkpoint inhibitors. The scientific rationale for these clinical trials is based on the findings from preclinical studies suggesting that RT can serve as an *in situ* vaccine to augment the effects of immunotherapy and a few case reports showing impressive clinical responses to such combinations. However, limited preclinical or clinical data are available to guide the selection of the radiation dose, fractionation schedule, and site to optimally synergize with immunotherapy. We initiated the present prospective specimen banking study with a goal of refining our understanding the systemic immune response to SAR monotherapy and how the response differs according to the site irradiated. To the best of our knowledge, no previous studies in patients have directly compared the systemic immune response in patients after SAR to different organs.

A few key studies characterize the immune changes after SAR in the setting of concurrent immunotherapy. Tang et al (42) reported that patients who received liver-directed SAR in conjunction with the CTLA-4 inhibitor ipilimumab had enhanced peripheral T-cell activation (as assessed by expression of ICOS, GITR, and 4-1BB) compared with patients who had undergone lung-directed SAR. Hiniker et al (26) identified an increase in peripheral IL-2–producing $CD8^+$ T cells and central memory T cells after RT in patients who responded to response to CTLA-4 inhibition and SAR. Postow et al (25) reported detailed immunoprofiling of a patient with progressive melanoma on CTLA-4 blockade who subsequently developed a systemic response after palliative RT and noted an increase in $ICOS^+CD4^+$ T cells, NY-ESO-1–specific IFN-γ–producing $CD4^+$ T cells, and $HLA\text{-}DR^+CD14^+$ monocytes and a decrease in myeloid-derived suppressor cells (25).

In addition, studies have reported the systemic immunophenotype in patients with stage I or II non-small

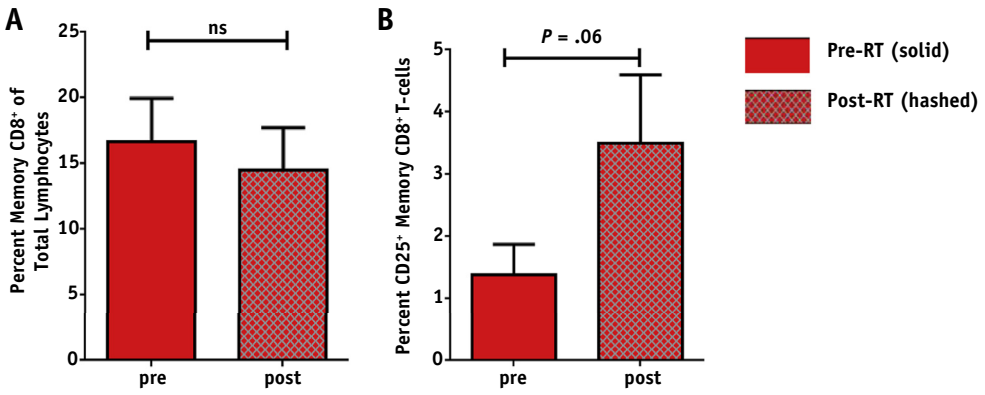

Fig. 4. Stereotactic ablative radiation therapy (RT; SAR) causes an increase in the percentage of activated $CD25^+$ memory $CD8^+$ T cells. (A) Percentage of $CD8^+$ memory T cells after SAR to parenchymal sites. (B) Percentage of activated $CD25^+$ memory $CD8^+$ T cells after SAR to parenchymal sites.

cell lung cancer (NSCLC) who received SAR alone. Maehata et al (28) described the peripheral immune changes that occur after SBRT for stage I NSCLC, showing that SBRT induces lymphopenia and decreased NK cell activity, which they attributed to RT directed to vertebral bone marrow in the SBRT field (28). Trovo et al (29) characterized cytokine changes after SBRT compared with conventional RT for early-stage NSCLC and found a mean reduction of IL-10 and IL-17 plasma levels. However, they did not consider individual immune cell subsets (29). Rutkowski et al (43) studied immune cell types after SBRT and observed an increase in the proportion of total $CD8^+$ T cells, total $CD4^+$ T cells, and $CD4^+$ T cells expressing GATA-3, T-bet, or ROR-γt and a decrease in $CD4^+Foxp3^+$ regulatory T cells (43). However, their study did not evaluate NK cells (43). All these studies examined the immune phenotype after SBRT to the lung alone. To the best of our knowledge, no studies have directly compared the peripheral immune response after SAR to different organs in the absence of concurrent immunotherapy.

We hypothesized that differences in T-cell and NK-cell activation after RT to different sites might relate to differences in the degree and potency of immunosuppression of the target tissue. Some proof of this phenomenon has been found in preclinical studies, which showed that intracranial melanoma produces more functional exhaustion and impairment of T-cell effector function compared with subcutaneous disease with the same tumor histologic type (44). To address this question, we focused on the unique tissue microenvironments that characterize the brain, bone, lung, and liver. The brain is characterized by the blood−brain barrier, which sequesters lymphocytes during steady state, creating a relatively "immunoprivileged site," but allows lymphocytes to transverse the cerebral vasculature during pathologic states (45). The bone marrow contains the perivascular hematopoietic stem cell niche, which contains mesenchymal stem cells and is characterized by hypoxia. The bone marrow also contains osteoclasts, involved in bone reabsorption, and osteoblasts, involved in bone remodeling (35, 46-48). In contrast, the lung is in constant contact with toxins and pathogens from the environment during respiration, and bronchial epithelial cells interact with innate immune cells, including plasmacytoid dendritic cells, alveolar macrophages, and NK cells, which promote immune tolerance (49). Similarly, the liver is constantly exposed to antigens transported from the colon by the portal vein and, therefore is composed of an abundance of innate immune cells, such as NK cells, γδ T cells, and Kupffer cells, which also contribute to immune tolerance (33). Both the lung and liver develop immune tolerance to most of the antigenic load delivered by air exchange or the portal venous blood supply (33, 50). Given the differences in blood supply, antigenic load, and relative abundance of innate immune cells and lymphocytes between these organs, we hypothesized that SAR delivered to these immunotolerant organs would differ from that of immunoprivileged organs such as the brain.

Owing to the abundance of NK cells in the lung and liver, we hypothesized that these innate immune cells would play a role in the response to SAR in these organs. Although NK cells do not express antigen receptors, they play important roles in viral infections and antitumor immunity by cytotoxic killing or the release of IFN-γ. In humans, 2 populations of NK cells can be distinguished by CD56 expression (51, 52). $CD56^{dim}$ cells that express CD16 (the low-affinity receptor for IgG, FcRγIII) have enhanced cytotoxicity, and $CD56^{hi}$ NK cells that do not express CD16 ($CD56^{hi}CD16^-$ cells) are able to secrete large amounts of IFN-γ, granulocyte-macrophage colony-stimulating factor, and TNF-α (53). Our results showed a decrease in both total NK cells and cytotoxic NK cells after SAR to these parenchymal sites. The decrease in NK cells in the peripheral blood after SAR to the parenchymal organs could represent increased homing or migration of NK cells to the irradiated tumor site. Previous work in our laboratory using a patient-derived xenograft model demonstrated a decreased tumor volume and

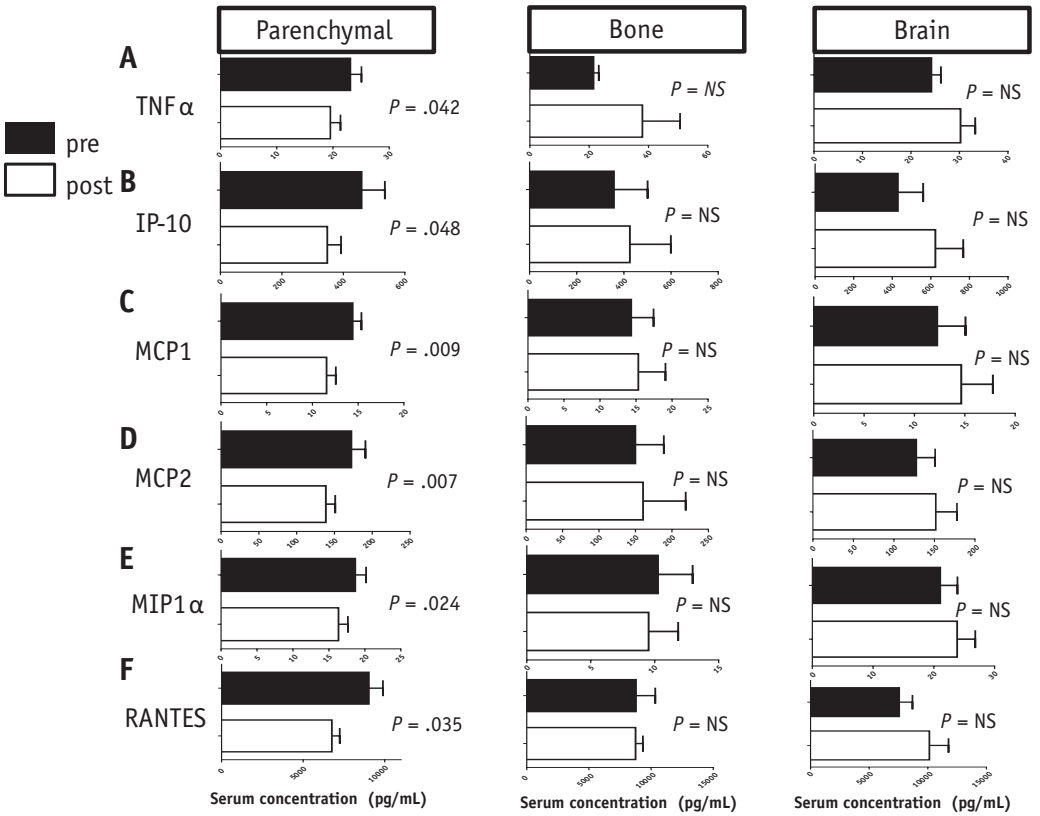

Fig. 5. Luminex analysis of cytokines and chemokines in the serum of patients treated with stereotactic ablative radiation therapy (SAR) to parenchymal, bone, and brain sites. (A) Tumor necrosis factor-α (TNF-α). (B) Inducible protein-10 (IP-10). (C) MCP-1. (D) MCP-2. (E) MIP-1α. (F) RANTES. (All cytokine and chemokine concentrations given in pg/mL.).

increased survival of PDX-bearing mice treated with a combination of RT and autologous NK cell-adoptive therapy (54). Tumor irradiation in this model leads to tumor cell upregulation of stress ligands such as NKG2D, which activate NK cells and increase homing and infiltration of tagged NK cells into the tumor (54). These findings suggest that the decrease in systemic NK cells after SAR identified in the present study might be secondary to increased NK cell homing to the tumor site. However, we cannot exclude the possibility that the decrease in NK cells seen in the peripheral blood of patients in our study might represent a systemic depletion of NK cells from both the irradiated organs and the peripheral blood.

TIM3 was initially identified as a T-helper 1-specific protein involved in regulating T-cell responses; however, the greatest expression of TIM3 was found on human NK cells. We saw an increase in circulating $TIM3^+$ NK cells after SAR to the parenchymal sites. Previous studies on $TIM3^+$ NK cells focused on their role as exhausted NK cells in several cancers, including melanoma and colorectal cancer (55, 56). Although previous studies have shown that the presence of these cells is associated with worse responses to therapies such as surgery (56), $TIM3^+$ NK cells have never been linked to RT. In aggregate, our data have shown that a decrease occurs in NK cells in the periphery after SAR but an increase in the $TIM3^+$ NK cell subset. Future studies will examine the mechanism by which SAR induces NK cell exhaustion and whether anti-TIM3 antibodies could be used to reverse NK cell exhaustion after RT.

Given the importance of T cells in the induction of the "abscopal" response, we investigated the role of SAR in the induction of memory T-cell response. We found an increase in $CD4^+$ memory T cells after SAR to parenchymal sites, with increased expression of ICOS and CD25 activation markers on these cells. ICOS is a T-cell specific cell surface activation and costimulatory molecule structurally related to CD28 and CTLA-4 that increases the proliferation and survival of activated $CD4^+$ effector memory T cells (42). Anti−CTLA-4 therapy (ipilimumab) increases the frequency of $CD4^+$ T cells expressing ICOS, and these effector T cells produce IFN-γ (57). This results from the increased signaling through the phosphinositide-3-kinase pathway and an increase in the expression of T-bet (58). An increased frequency of $ICOS^+CD4^+$ T cells has been associated with improved clinical outcomes for anti−CTLA-4 and anti-OX40 immunotherapies (57, 59). Importantly, this population is not induced by anti−programmed cell death ligand 1 (PD-L1) therapy and might represent a distinct mechanistic pathway of anti-tumor immunity (60). Our recent clinical data presented here have demonstrated that this cell population is also

upregulated after SBRT. Therefore, it is possible that activation of $ICOS^+CD4^+$ T cells might represent a novel, but synergistic, immune mechanism such that SBRT could enhance PD-L1 checkpoint inhibition.

Unexpectedly, we did not observe any differences in $PD\text{-}1^+$ expression on any T-cell subsets and did not observe any difference in $Foxp3^+$ regulatory T cells. This could have been because PD-1 is upregulated on antigen-specific T cells, and we were only able to quantify differences in the entire memory T-cell population rather than the antigen-specific T cells in our patient samples. However, studies have reported that PD-1, PD-L1, and T-regulatory cell markers are decreased after cryopreservation of human PBMCs (61, 62); therefore, it is possible that our negative findings resulted from the limitations of our experimental protocol.

Our Luminex analysis revealed a systemic decrease in TNF-α and a decrease in multiple chemokines such as RANTES (CCL5) and IP-10 (CXCL10). RANTES plays a role in homing and migration of effector and memory T cells and helps sustain CD8 T-cell responses during a systemic chronic viral infection (63); therefore, it is possible that it plays a similar role in the antitumor immunity induced by SAR. IP-10 is IFN-γ–inducible protein 10 and is a chemoattractant for activated memory T cells and NK cells by binding to and activating CXCR3 (64). Therefore, it might play a role in T-cell or NK-cell homing after SAR. The systemic decrease in these cytokines is somewhat unexpected given the inflammatory nature of RT but has been reported in other studies (65). The clinical significance of these decreases and how they relate to the changes that might be occurring in the tumor microenvironment are unclear. Future studies are needed to determine whether this results from the reduced half-life, increased degradation, or lower transcription and translation of these cytokines. Unexpectedly, we did not observe changes in the proinflammatory cytokines IFN-α, IFN-γ, or TGF-β, which have been implicated in immune response to RT in other studies, perhaps because the changes in these cytokines are short lived (22-24, 66).

Our study had several key limitations, most significantly the inherent baseline differences in radiation dose, fractionation, and target volume size used to treat the parenchymal sites compared with the bony metastases and brain metastases owing to the standard of care treatment for each disease site. It is possible the observed differences in immunophenotype resulted from differences in dose and fractionation, rather than differences in the treated site. The Spearman correlation coefficients suggested that greater total doses of ablative RT are associated with an increase in the percentage of activated memory $CD4^+$ and $CD8^+$ T cells. The ablative doses used to irradiate each site are site dependent, and higher total doses are typically used clinically for liver and lung tumors than for brain and bone tumors. Therefore, the observed differences in immune cell populations between the sites could have been because the parenchymal lesions were treated to a higher ablative dose than were the bone and brain lesions. We could not analyze the contribution of these 2 variables separately because the study had a limited sample size, and all patients were treated according to the standard of care SAR protocols, which allowed for minimal variation in the dose within each site. An additional limitation was that all our analyses were performed on batched cryopreserved PBMCs, and some data have suggested that some biomarkers might be altered in cryopreserved samples (61, 62).

Conclusions

We have identified changes in systemic immunophenotype after SAR to the lung and liver that we did not observe after SAR to the bone and brain. Our findings suggest SAR might be less immunomodulatory when directed to the bone or brain, possibly because of the immunosuppressive environment in these organs. We could not exclude the possibility that differences in the standard-of-care dose schemas for these organs contributed to the observed differences. The correlation between systemic immunophenotype changes and patient outcomes will be crucial to understanding the clinical relevance of our findings and the potential for any of these changes to serve as biomarkers. Ultimately, our goal is to use this knowledge about the immune response after SAR to different sites to refine ongoing and future clinical studies combining SAR and immunotherapy.

References

1. Timmerman R. Stereotactic body radiation therapy for inoperable early stage lung cancer. *JAMA* 2010;303:1070-1076.
2. Chi A, Liao Z, Nguyen NP, et al. Systemic review of the patterns of failure following stereotactic body radiation therapy in early-stage non-small-cell lung cancer: Clinical implications. *Radiother Oncol* 2010;94:1-11.
3. Siva S, Slotman BJ. Stereotactic ablative body radiotherapy for lung metastases: Where is the evidence and what are we doing with it? *Semin Radiat Oncol* 2017;27:229-239.
4. Su T-S, Liang P, Liang J, et al. Long-term survival analysis of stereotactic ablative radiotherapy versus liver resection for small hepatocellular carcinoma. *Int J Radiat Oncol* 2017;98:639-646.
5. Gkika E, Schultheiss M, Bettinger D, et al. Excellent local control and tolerance profile after stereotactic body radiotherapy of advanced hepatocellular carcinoma. *Radiat Oncol* 2017;12:116.
6. Chance WW, Nguyen Q-N, Mehran R, et al. Stereotactic ablative radiotherapy for adrenal gland metastases: Factors influencing outcomes, patterns of failure, and dosimetric thresholds for toxicity. *Pract Radiat Oncol* 2017;7:e195-e203.
7. Ricardi U, Badellino S, Filippi AR. Clinical applications of stereotactic radiation therapy for oligometastatic cancer patients: A disease-oriented approach. *J Radiat Res* 2016;57(Suppl. 1):i58-i68.
8. Formenti SC, Demaria S. Systemic effects of local radiotherapy. *Lancet Oncol* 2009;10:718-726.
9. Formenti SC, Demaria S. Radiation therapy to convert the tumor into an in situ vaccine. *Int J Radiat Oncol* 2012;84:879-880.
10. Weichselbaum RR, Liang H, Deng L, et al. Radiotherapy and immunotherapy: A beneficial liaison? *Nat Rev Clin Oncol* 2017;14:365-379.

11. Baird JR, Monjazeb AM, Shah O, et al. Stimulating innate immunity to enhance radiation therapy-induced tumor control. *Int J Radiat Oncol* 2017;99:362-373.
12. Young KH, Baird JR, Savage T, et al. Optimizing timing of immunotherapy improves control of tumors by hypofractionated radiation therapy. *PLoS One* 2016;11:e0157164.
13. Sharabi AB, Lim M, DeWeese TL, et al. Radiation and checkpoint blockade immunotherapy: Radiosensitisation and potential mechanisms of synergy. *Lancet Oncol* 2015;16:e498-e509.
14. Crittenden M, Kohrt H, Levy R, et al. Current clinical trials testing combinations of immunotherapy and radiation. *Semin Radiat Oncol* 2015;25:54-64.
15. Formenti SC, Demaria S. Combining radiotherapy and cancer immunotherapy: A paradigm shift. *J Natl Cancer Inst* 2013;105:256-265.
16. Apetoh L, Ghiringhelli F, Tesniere A, et al. Toll-like receptor 4—dependent contribution of the immune system to anticancer chemotherapy and radiotherapy. *Nat Med* 2007;13:1050-1059.
17. Obeid M, Tesniere A, Ghiringhelli F, et al. Calreticulin exposure dictates the immunogenicity of cancer cell death. *Nat Med* 2007;13:54-61.
18. Lee Y, Auh SL, Wang Y, et al. Therapeutic effects of ablative radiation on local tumor require CD8+ T cells: Changing strategies for cancer treatment. *Blood* 2009;114:589-595.
19. Klug F, Prakash H, Huber PE, et al. Low-dose irradiation programs macrophage differentiation to an iNOS+/M1 phenotype that orchestrates effective T cell immunotherapy. *Cancer Cell* 2013;24:589-602.
20. Wu C-Y, Yang L-H, Yang H-Y, et al. Enhanced cancer radiotherapy through immunosuppressive stromal cell destruction in tumors. *Clin Cancer Res* 2014;20:644-657.
21. Crocenzi T, Cottam B, Newell P, et al. A hypofractionated radiation regimen avoids the lymphopenia associated with neoadjuvant chemoradiation therapy of borderline resectable and locally advanced pancreatic adenocarcinoma. *J Immunother Cancer* 2016;4:45.
22. Vanpouille-Box C, Alard A, Aryankalayil MJ, et al. DNA exonuclease Trex1 regulates radiotherapy-induced tumour immunogenicity. *Nat Commun* 2017;8:15618.
23. Deng L, Liang H, Xu M, et al. STING-dependent cytosolic DNA sensing promotes radiation-induced type I interferon-dependent antitumor immunity in immunogenic tumors. *Immunity* 2014;41:843-852.
24. Dewan MZ, Galloway AE, Kawashima N, et al. Fractionated but not single-dose radiotherapy induces an immune-mediated abscopal effect when combined with anti-CTLA-4 antibody. *Clin Cancer Res* 2009;15:5379-5388.
25. Postow MA, Callahan MK, Barker CA, et al. Immunologic correlates of the abscopal effect in a patient with melanoma. *N Engl J Med* 2012;366:925-931.
26. Hiniker SM, Reddy SA, Maecker HT, et al. A prospective clinical trial combining radiation therapy with systemic immunotherapy. *Int J Radiat Oncol Biol Phys* 2016;96:578-588.
27. Golden EB, Demaria S, Schiff PB, et al. An abscopal response to radiation and ipilimumab in a patient with metastatic non-small cell lung cancer. *Cancer Immunol Res* 2013;1:365-372.
28. Maehata Y, Onishi H, Kuriyama K, et al. Immune responses following stereotactic body radiotherapy for stage I primary lung cancer. *Biomed Res Int* 2013;2013:1-11.
29. Trovo M, Giaj-Levra N, Furlan C, et al. Stereotactic body radiation therapy and intensity modulated radiation therapy induce different plasmatic cytokine changes in non-small cell lung cancer patients: A pilot study. *Clin Transl Oncol* 2016;18:1003-1010.
30. Gustafson MP, Bornschlegl S, Park SS, et al. Comprehensive assessment of circulating immune cell populations in response to stereotactic body radiation therapy in patients with liver cancer. *Adv Radiat Oncol* 2017;2:540-547.
31. Wild AT, Herman JM, Dholakia AS, et al. Lymphocyte-sparing effect of stereotactic body radiation therapy in patients with unresectable pancreatic cancer. *Int J Radiat Oncol* 2016;94:571-579.
32. Muraro E, Furlan C, Avanzo M, et al. Local high-dose radiotherapy induces systemic immunomodulating effects of potential therapeutic relevance in oligometastatic breast cancer. *Front Immunol* 2017;8:1476.
33. Sun H, Sun C, Tian Z, et al. NK cells in immunotolerant organs. *Cell Mol Immunol* 2013;10:202-212.
34. Pardee AD, Butterfield LH. Immunotherapy of hepatocellular carcinoma. *Oncoimmunology* 2012;1:48-55.
35. Méndez-Ferrer S, Michurina TV, Ferraro F, et al. Mesenchymal and haematopoietic stem cells form a unique bone marrow niche. *Nature* 2010;466:829-834.
36. Rasid O, Ciulean IS, Fitting C, et al. Local microenvironment controls the compartmentalization of NK cell responses during systemic inflammation in mice. *J Immunol* 2016;197:2444-2454.
37. Lepone LM, Donahue RN, Grenga I, et al. Analyses of 123 peripheral human immune cell subsets: Defining differences with age and between healthy donors and cancer patients not detected in analysis of standard immune cell types. *J Circ Biomarkers* 2016;5:5.
38. Donahue RN, Lepone LM, Grenga I, et al. Analyses of the peripheral immunome following multiple administrations of avelumab, a human IgG1 anti-PD-L1 monoclonal antibody. *J Immunother Cancer* 2017;5:20.
39. Baumgarth N, Roederer M. A practical approach to multicolor flow cytometry for immunophenotyping. *J Immunol Methods* 2000;243:77-97.
40. Michie CA, McLean A, Alcock C, et al. Lifespan of human lymphocyte subsets defined by CD45 isoforms. *Nature* 1992;360:264-265.
41. Sallusto F, Lenig D, Förster R, et al. Two subsets of memory T lymphocytes with distinct homing potentials and effector functions. *Nature* 1999;401:708-712.
42. Tang C, Welsh JW, de Groot P, et al. Ipilimumab with stereotactic ablative radiation therapy: Phase I results and immunologic correlates from peripheral T cells. *Clin Cancer Res* 2017;23:1388-1396.
43. Rutkowski J, Ślebioda T, Kmieć Z, et al. Changes of systemic immune response after stereotactic ablative radiotherapy (SABR)—First results of a prospective study in early lung cancer patients. *Polish Arch Intern Med* 2017;127:245-253.
44. Jackson CM, Kochel CM, Nirschl CJ, et al. Systemic tolerance mediated by melanoma brain tumors is reversible by radiotherapy and vaccination. *Clin Cancer Res* 2016;22:1161-1172.
45. Louveau A, Harris TH, Kipnis J. Revisiting the mechanisms of CNS immune privilege. *Trends Immunol* 2015;36:569-577.
46. Bussard KM, Gay CV, Mastro AM. The bone microenvironment in metastasis: What is special about bone? *Cancer Metastasis Rev* 2008;27:41-55.
47. Takubo K, Goda N, Yamada W, et al. Regulation of the HIF-1α level is essential for hematopoietic stem cells. *Cell Stem Cell* 2010;7:391-402.
48. Morrison SJ, Scadden DT. The bone marrow niche for haematopoietic stem cells. *Nature* 2014;505:327-334.
49. Bals R, Hiemstra PS. Innate immunity in the lung: How epithelial cells fight against respiratory pathogens. *Eur Respir J* 2004;23:327-333.
50. Lau AH, Thomson AW. Dendritic cells and immune regulation in the liver. *Gut* 2003;52:307-314.
51. Di Santo JP. Natural killer cells: Diversity in search of a niche. *Nat Immunol* 2008;9:473-475.
52. Lanier LL, Le AM, Civin CI, et al. The relationship of CD16 (Leu-11) and Leu-19 (NKH-1) antigen expression on human peripheral blood NK cells and cytotoxic T lymphocytes. *J Immunol* 1986;136:4480-4486.
53. Cooper MA, Fehniger TA, Caligiuri MA. The biology of human natural killer-cell subsets. *Trends Immunol* 2001;22:633-640.
54. Ames E, Canter RJ, Grossenbacher SK, et al. Enhanced targeting of stem-like solid tumor cells with radiation and natural killer cells. *Oncoimmunology* 2015;4:e1036212.

55. da Silva IP, Gallois A, Jimenez-Baranda S, et al. Reversal of NK-cell exhaustion in advanced melanoma by TIM-3 blockade. *Cancer Immunol Res* 2014;2:410-422.
56. Wang Y, Sun J, Gao W, et al. Preoperative TIM-3 expression on peripheral NK cells is correlated with pathologic TNM staging in colorectal cancer. *Mol Med Rep* 2017;15:3810-3818.
57. Ng Tang D, Shen Y, Sun J, et al. Increased frequency of ICOS+ CD4 T cells as a pharmacodynamic biomarker for anti-CTLA-4 therapy. *Cancer Immunol Res* 2013;1:229-234.
58. Chen H, Fu T, Suh W-K, et al. CD4 T cells require ICOS-mediated PI3K signaling to increase T-Bet expression in the setting of anti-CTLA-4 therapy. *Cancer Immunol Res* 2014;2:167-176.
59. Metzger TC, Long H, Potluri S, et al. ICOS promotes the function of CD4+ effector T cells during anti-OX40-mediated tumor rejection. *Cancer Res* 2016;76:3684-3689.
60. Wei SC, Levine JH, Cogdill AP, et al. Distinct cellular mechanisms underlie anti-CTLA-4 and anti-PD-1 checkpoint blockade. *Cell* 2017;170:1120-1133.e17.
61. Sattui S, de la Flor C, Sanchez C, et al. Cryopreservation modulates the detection of regulatory T cell markers. *Cytom Part B Clin Cytom* 2012;82B:54-58.
62. Campbell DE, Tustin NB, Riedel E, et al. Cryopreservation decreases receptor PD-1 and ligand PD-L1 coinhibitory expression on peripheral blood mononuclear cell-derived T cells and monocytes. *Clin Vaccine Immunol* 2009;16:1648-1653.
63. Crawford A, Angelosanto JM, Nadwodny KL, et al. A role for the chemokine RANTES in regulating CD8 T cell responses during chronic viral infection. *PLoS Pathog* 2011;7:e1002098.
64. Dufour JH, Dziejman M, Liu MT, et al. IFN-gamma-inducible protein 10 (IP-10; CXCL10)-deficient mice reveal a role for IP-10 in effector T cell generation and trafficking. *J Immunol* 2002;168:3195-3204.
65. Sridharan V, Margalit DN, Lynch SA, et al. Definitive chemo-radiation alters the immunologic landscape and immune checkpoints in head and neck cancer. *Br J Cancer* 2016;115:252-260.
66. Vanpouille-Box C, Diamond JM, Pilones KA, et al. TGF is a master regulator of radiation therapy-induced antitumor immunity. *Cancer Res* 2015;75:2232-2242.